Journal of Structural Geology 33 (2011) 1302–1311

Contents lists available at ScienceDirect

Journal of Structural Geology

journal homepage: www.elsevier.com/locate/jsg

Riedel shear structures in the co-seismic surface rupture zone produced by the 2001 M_w 7.8 Kunlun earthquake, northern Tibetan Plateau

Aiming Lin*, Masayuki Nishikawa

Graduate School of Science and Technology, Shizuoka University, Shizuoka 422-8529, Japan

ARTICLE INFO

Article history:
Received 5 November 2010
Received in revised form
16 June 2011
Accepted 17 July 2011
Available online 22 July 2011

Keywords:
Riedel shear structure
Co-seismic surface rupture
Strike-slip Kunlun fault
2001 M_w 7.8 Kunlun earthquake
Tibetan plateau

ABSTRACT

We present a case study of Riedel shear structures related to the co-seismic surface ruptures produced during the 2001 M_w 7.8 Kunlun earthquake in northern Tibet, which are related to strike-slip movement along the Kunlun Fault. Field investigations and interpretations of high-resolution remote sensing images show that the 2001 co-seismic surface ruptures, striking WNW–ESE, are mainly characterized by Riedel shear structures, including *T* fractures, and *R, Y,* and *P* shears. A left-lateral shear sense is indicated. To assess the Riedel shear fabrics quantitatively, we measured the azimuth of 19,455 co-seismic surface rupture strands, the width of rupture zones at 474 profiles, and 336 fold axes of mole track structures, using 1-m-resolution IKONOS and 0.61-m-resolution QuickBird images acquired soon after the earthquake. The analytical results show that i) the co-seismic surface ruptures are generally concentrated in up to five subparallel sub-rupture zones, with individual sub-rupture zones varying in width from 3 to 350 m (generally <100 m); ii) the total width across all sub-rupture zones is generally <500 m (though locally >1–2 km); iii) *T* fractures are mainly developed within the alluvial deposits at counterclockwise angles of 15–40° relative to the general trend of the rupture zone; iv) *P* shears are also mainly found in the alluvial deposits, but at counterclockwise to clockwise angles of 5–10° relative to the general trend; and v) *Y* and *R* shears are developed within both the alluvial deposits and basement rocks, mainly representing the reactivation of pre-existing fault traces. The results demonstrate that the co-seismic Riedel shear structures are primarily controlled by the local geology during surface rupture formation, consistent with the idea that Riedel shear structures are common fault patterns within strike-slip shear zones and that their development is related to the early stages of fault evolution.

1. Introduction

Most large earthquakes are the result of slip on pre-existing active faults (e.g., Yeats et al., 1997; Lin et al., 2003, 2009). The slip often results in a ground deformation causing surface ruptures; therefore, an investigation of the processes of seismic faulting requires information on the structure of rupture zones and the nature of seismogenic faults (e.g., Lin et al., 2002, 2003, 2009, 2011). Geological and geophysical data show that co-seismic surface ruptures not only reflect the ground surface morphology of the fault, but also provide an indication of the structural characteristics of the fault at depth, as well as the pre-existing tectonic environment (e.g., King, 1986; Lin et al., 2001, 2003, 2009). Consequently, a study of the surface geometric structures in a co-seismic shear zone would provide new insights into the rupturing behavior and mechanical properties of seismogenic faults.

The geometric features of strike-slip faults are generally characterized by Riedel shear structures clearly shown at the surface, as exemplified in experiments (e.g., Tchalenko, 1968, 1970) and in the field as co-seismic surface ruptures (e.g., Tchalenko and Ambraseys, 1970; Lin and Uda, 1996; Lin et al., 2002, 2003; Angelier et al., 2004). However, the lack of quantitative analytical data and a limited number of case studies hinders further understanding of the geometric patterns of co-seismic shear structures and the rupturing mechanics of seismogenic faults. The 2001 M_w 7.8 Kunlun earthquake produced a surface rupture zone extending 450 km along the pre-existing strike-slip Kunlun Fault (Lin et al., 2002, 2003, 2004; Lin and Nishikawa, 2007), and this rupture zone provides us with a rare opportunity to study the shear zone structures of surface ruptures produced by a large intracontinental earthquake.

We have previously carried out a series of studies on the rupture processes, the temporal and spatial distributions of strike-slip

* Corresponding author. Institute of Geosciences, Shizuoka University, Ohya 832, Shizuoka 422-8529, Japan. Fax: +81 54 238 4792.
E-mail address: slin@ipc.shizuoka.ac.jp (A. Lin).

0191-8141/$ – see front matter © 2011 Elsevier Ltd. All rights reserved.
doi:10.1016/j.jsg.2011.07.003

displacements, and the geometric structures of co-seismic surface ruptures produced by the 2001 M_w 7.8 Kunlun earthquake (Lin et al., 2002, 2003, 2004; Fu and Lin, 2003). In addition, we have investigated slip rates and the recurrence intervals of large earthquakes on the Kunlun Fault (Guo et al., 2006, 2007; Lin et al., 2006; Lin and Nishikawa, 2007; Lin and Guo, 2008, 2009). Our previous studies demonstrated that the 2001 Kunlun earthquake was characterized by a pure strike-slip mechanism, and that the distribution patterns of temporal and spatial strike-slip displacements and rupture processes were controlled mainly by pre-existing geological structures associated with the strike-slip Kunlun Fault.

For this study, we focus on the co-seismic Riedel shear structures developed in the 450-km-long co-seismic surface rupture zone produced by the 2001 M_w 7.8 Kunlun earthquake, and discuss the relationships between the co-seismic Riedel shear structures and the pre-existing active strike-slip Kunlun Fault. Our results are based on field investigations and interpretations of 1-m-resolution IKONOS and 0.61-m-resolution QuickBird images.

2. Tectonic setting

The Kunlun Fault strikes E–W to WNW–ESE for ~1200 km in the eastern-central Kunlun mountain range, northern Tibet (Fig. 1). The average elevation is ~4500 m. The fault is one of the major strike-slip active faults on the Tibetan Plateau, and it plays an important role in accommodating the eastwards extrusion of the Tibetan Plateau caused by the ongoing continental collision between the Indian and Eurasian Plates (e.g., Molnar and Tapponnier, 1975; Tapponnier et al., 2001; Lin and Guo, 2008).

More than 10 moderate to large ($M \geq 6.0$) earthquakes have occurred on the Kunlun Fault over the last century, with three $M \geq 7.5$ events producing distinct surface rupture deformation structures, indicating that the fault is currently active as a seismogenic fault (e.g., International Seismological Centre, 2001; Lin et al., 2002, 2003). The 1937 M 7.5 Tuosuo Lake earthquake resulted in rupturing in the eastern segment (Jia et al., 1988; Guo et al., 2007). The1997 M_w 7.6 Manyi earthquake occurred at the western extremity of the fault (Peltzer et al., 1999).

More recently, the 2001 M_w 7.8 Kunlun earthquake resulted in rupturing within the central-western segment of the fault, between the co-seismic surface rupture zones of the 1937 and 1997 events (Lin et al., 2002, 2003, 2006). This earthquake produced a surface rupture that extends for 400–450 km, and a strike-slip displacement of up to about 16 m (average 3–8 m) along the western segment of the Kunlun Fault (Lin et al., 2002, 2003, 2004; Lin and Nishikawa, 2007). Based on its morphological characteristics, the geological structures, and the displacement distributions, the 2001 surface rupture zone can be divided into the following four distinct segments (from west to east): the Buka Daban Peak (BDP), Hongshui River (HR), Kusai Lake (KL), and Kunlun Pass (KP) segments (Fig. 1; Lin et al., 2003).

Palaeoseismic studies show that the average recurrence interval of large-magnitude earthquakes ranges from 300 to 400 years in the western segment of the fault (Lin et al., 2006; Lin and Guo, 2009), and up to 1000 years in the eastern segment (Lin and Guo, 2008). These studies have shown that the slip rate along the Kunlun Fault is non-uniform, and that it diminishes from 10 to 20 mm/yr in the west to 2–3 mm/yr in the east, with an average gradient of 1 mm/100 km (Lin and Guo, 2008). These figures are consistent with GPS observations (Zhang et al., 2004).

3. Analytical methods

In the field, it proved difficult to map all the surface rupture strands along the 450-km-long rupture zone immediately after the 2001 M_w Kunkun earthquake, because of the remoteness and extreme height of this mountainous region, the bad weather conditions, and the snow, glaciers, and moraine, which not only make access difficult, but shorten the time available each day in which it is possible to work. Furthermore, some of the co-seismic surface rupture traces are subjected to rapid erosion as a result of rain and freeze–thawing processes.

A possible solution to these problems of collecting data directly in the field is remote sensing, using high-resolution imagery data such as the 1-m-resolution IKONOS and 0.61-m-resolution QuickBird images acquired soon after the earthquake. The high elevation of the Tibetan Plateau, the lack of vegetation, and the absence of human modification of the ground surface makes this an ideal region for using remote sensing images to analyze co-seismic ruptures produced by large earthquakes. In our previous studies, we successfully used remote sensing images to measure the amounts of strike-slip and the strand lengths of co-seismic surface ruptures along the 450 km-long surface rupture zone (Lin et al., 2003, 2004; Lin and Nishikawa, 2007).

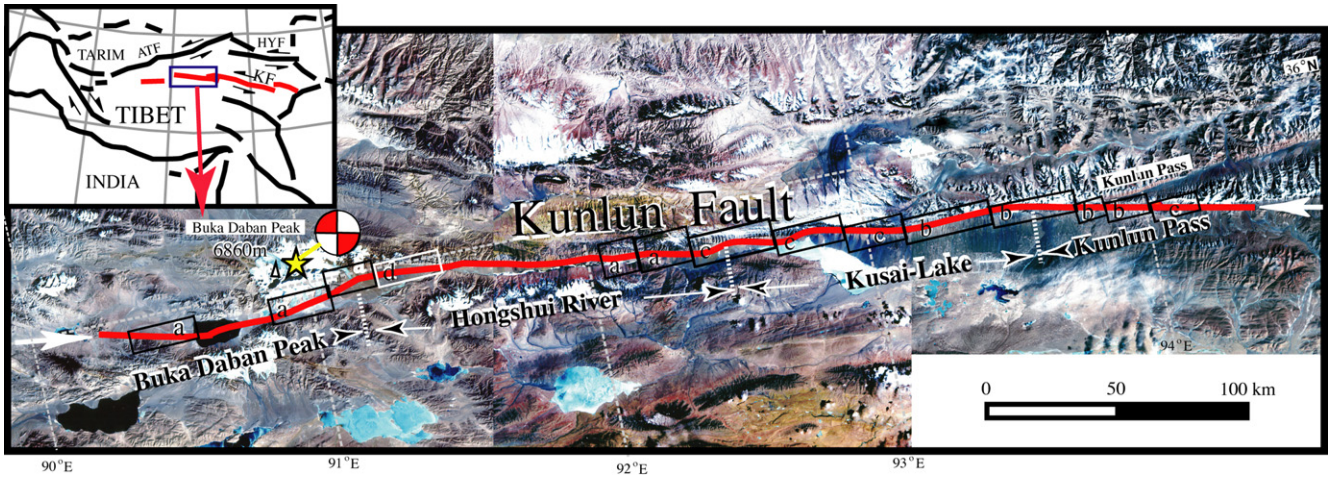

Fig. 1. Index map and satellite image showing the Kunlun Fault (white arrows), which was activated during the 2001 M_w 7.8 Kunlun earthquake, and the areas covered by IKONOS (black rectangles) and QuickBird (white rectangles) images (modified from Lin et al., 2002, 2003). ATF: Altyn Tagh Fault; HYF: Haiyuan Fault; KF: Kunlun Fault. The star indicates the epicenter of the 2001 earthquake. *a*–*d* indicate the dates of image data acquisition: *a*: January 2002; *b*: March 2003; *c*: October 2002; and *d*: October 2003.

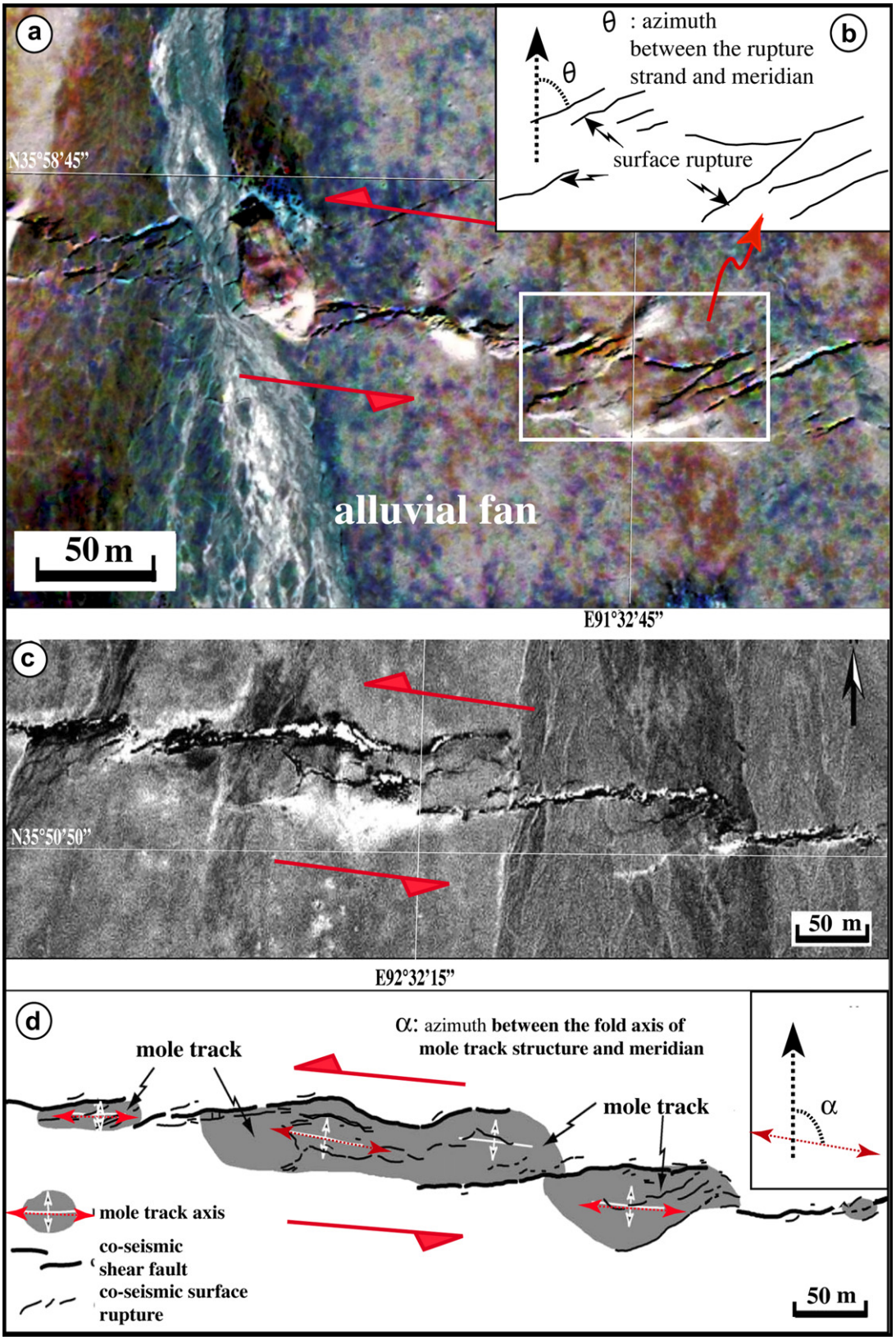

Fig. 2. Multispectral QuickBird (a) and IKONOS (c) images showing the co-seismic surface ruptures and mole structures. (a) Multispectral QuickBird image showing the right-hand en echelon pattern of co-seismic surface ruptures developed on alluvial fans. (b) Sketch showing the azimuth (θ) between a surface rupture strand and the meridian. (c) IKONOS image showing mole track structures and related surface ruptures. (d) Sketch of (c) showing the azimuth (α) between the fold axis of a mole track structure and the meridian (modified from Lin et al., 2004).

For the present study, we analyzed IKONOS and QuickBird images over a distance of about 300 km, to measure rupture zone widths and the strike of individual surface rupture strands (Fig. 1). The IKONOS images, containing longitude and latitude data, were acquired soon after the 2001 earthquake, in January, March, and October 2002, and the QuickBird data were acquired in October 2003 (Fig. 1). The strike of individual surface ruptures was determined using the readings of longitude and latitude at both ends of each single rupture.

The strand lengths of individual surface ruptures were recorded in our previous studies, and they range from <5 m to 200 m, with most in the range 5–50 m. For the present study, using large-scale images (up to 1:1000 scale), and on the basis of the readings of longitude and latitude at both ends of each surface rupture strand, we measured the azimuth of individual rupture strands and fold axes of mole track structure (Fig. 2).

The results of field investigations and analyses of high-resolution images show that the co-seismic surface ruptures are

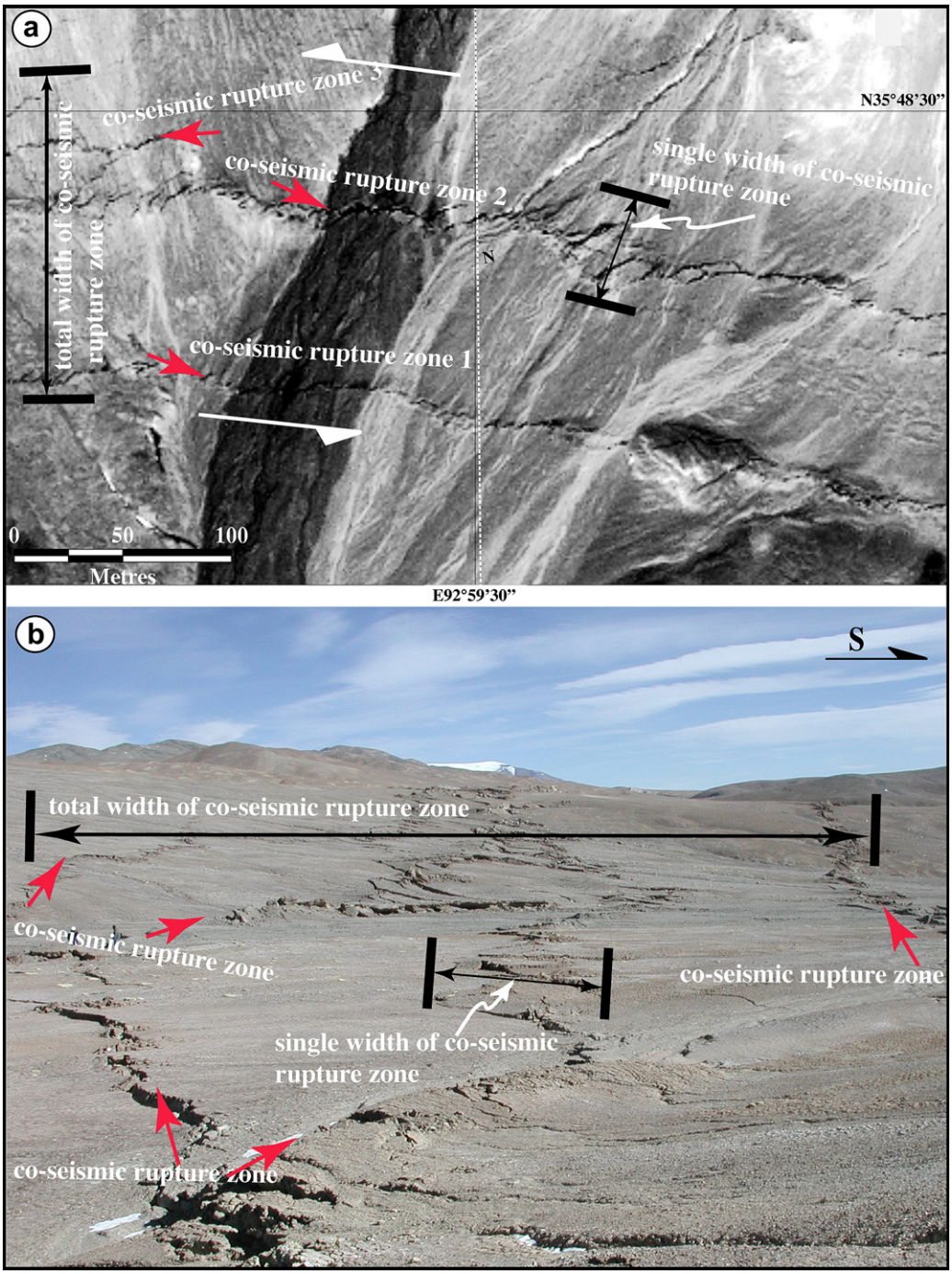

Fig. 3. IKONOS image (a) and field photograph (b) showing the deformation features of surface ruptures. (a) IKONOS image shows how the width of an individual sub-rupture zone and the overall width of an entire co-seismic surface rupture zone were measured. (b) Photograph showing the distribution patterns of the subparallel sub-rupture zones, as developed in the KL segment. Short red arrows indicate the sub-rupture zone. Long white arrows indicate the shear sense. (For interpretation of the references to colour in this figure legend, the reader is referred to the web version of this article.)

generally distributed in up to five subparallel sub-rupture zones (Fig. 3). When measuring the width of a surface rupture zone, we separately measured the width of individual sub-rupture zones as well as the total width across the rupture zone as a whole, and measurements were taken from profiles perpendicular to the general trend of each co-seismic surface rupture zone, as shown in Fig. 3.

4. Results

We measured the azimuth of 19,791 co-seismic rupture strands consisting of 19,455 surface rupture strands and 336 fold axes of mole track structures. To assist in understanding the relationships between the orientation of rupture strands and local geology, the measurements for the four surface rupture segments are plotted on

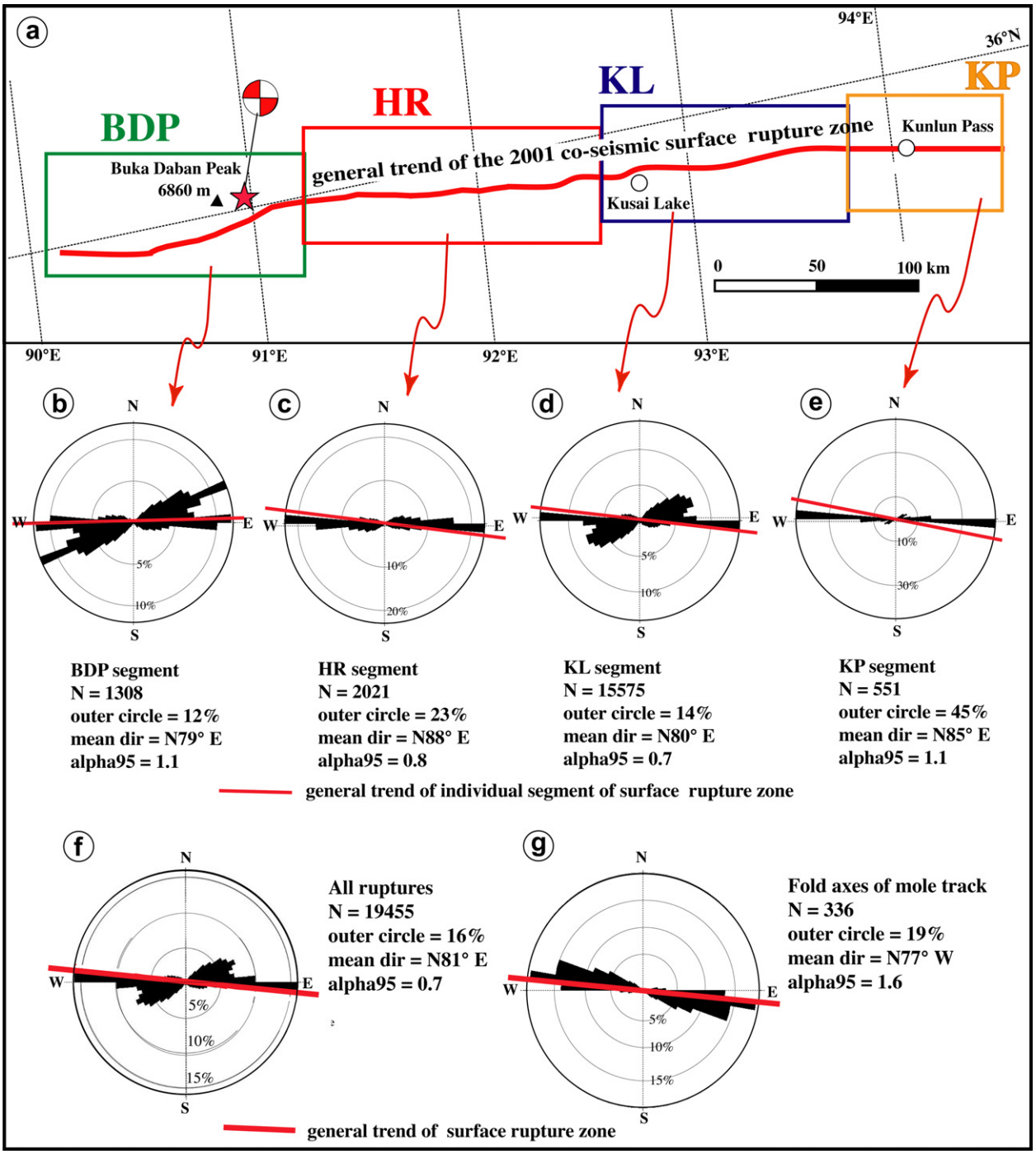

Fig. 4. Index map (a) and rose diagrams (b–g) showing the distribution of angles between individual rupture strands and the general trend of the rupture zone. (a) Index map showing the segments of the 2001 co-seismic surface rupture zone: BDP, Buka Daban Peak segment; HR, Hongshui River segment; KL, Kusai Lake segment; and KP, Kunlun Pass segment. The red star indicates the epicenter of the 2001 earthquake. (b–e) Rose diagrams showing the distribution of angles in the BDP, HR, KL, and KP segments, respectively. (f) Rose diagram showing the distribution of angles for all measured surface ruptures. (g) Rose diagram showing the orientation of the fold axes of mole track structures. See text for details. (For interpretation of the references to colour in this figure legend, the reader is referred to the web version of this article.)

four separate rose diagrams (Fig. 4b–e), and then compiled in a single diagram for the entire rupture zone (Fig. 4f). All the measurements of fold axes are plotted on a single rose diagram (Fig. 4g).

The results show that i) the co-seismic surface rupture strands are mainly within an angle of 0–40° from the general trend of the co-seismic surface rupture zone (Fig. 4f); ii) the fold axes of mole track structures are consistently oriented at lower angles ($< \pm 10°$) to the general trend of the whole rupture zone (Fig. 4g); and iii) the angle between the surface rupture strands and the general trend of individual sub-rupture zones varies from 0 to 40° in the BDP and KL segments to <10° in the HR and KP segments (Fig. 4b–e). The widths of individual sub-rupture zones and the total width of the entire rupture zone, composed of subparallel sub-rupture zones, were measured from 298 profiles across individual sub-ruptures, and from 176 profiles across the entire co-seismic surface rupture zone. The results show that most surface ruptures consist of up to five subparallel sub-rupture zones, where individual zones vary from 3 m to 350 m in width (generally <100 m) (Fig. 5a), and where the total width of the entire rupture zone is generally <500 m, although locally up to 1890 m (Fig. 5b). These results are consistent with those obtained directly in the field (Lin et al., 2002, 2003).

5. Discussion

5.1. Riedel shear structures in the co-seismic surface rupture zone

Since *Riedel shear* structures were first reported by Riedel (1929), they have been widely recognized as a fundamental part of the structure of shear zones associated with strike-slip displacements induced by large earthquakes (e.g., Tchalenko, 1970; Lin et al., 2001, 2002, 2003; Angelier and Bergerat, 2002, 2004; Rao et al., in press), basement faulting (e.g., Moore, 1979; Ahlgren, 2001; Katz et al., 2004), interplate shearing (Cunningham, 1993), and sand-box experiments (e.g., Tchalenko, 1970; Naylor et al., 1986). An idealized Riedel shear zone generally consists of conjugate *R* and *R'* shear fractures inclined at angles of $45° + \varphi/2$ and $45° - \varphi/2$ (where φ is the angle of internal friction of the host rock) to the general trend of the shear zone, a *P* shear inclined at an angle of $-45° - \varphi/2$, and a *T* fracture at an angle of approximately 45° (Fig. 6a) (e.g., Tchalenko, 1968; Bartlett et al., 1981; Ahlgren, 2001). The *R* and *P* shears are synthetic to the sense of slip along the shear zone, *R'* shears are antithetic, *T* fractures are purely tensional features, and *Y* shears are generally composed of discrete shear faults parallel to the general trend of the shear zone (Fig. 6) (Katz et al., 2004).

In the present study, the Riedel shear structures related to the 2001 co-seismic surface rupture zone were identified from high-resolution images (Figs. 2 and 7 a, b); they are also visible in the field (Fig. 7c–f). The deformation characteristics, angular relationships between individual rupture strands and the general trend of the surface rupture zone indicate that the 2001 co-seismic surface ruptures consist mainly of *R* and *Y* shears, *T* fractures (Figs. 4b–f and 6b), and *P* shears (Figs. 4g and 6c). There is a lack of *R'* shears. The orientation of surface rupture trends shows that *R*, *Y*, and *P* shears are commonly developed in all four co-seismic surface rupture segments, but *T* fractures are mainly found in the BDP and KL segments (Fig. 4b–e).

In natural shear systems, the angular relationships between individual shear surfaces and the principal shear zone vary according to a number of factors, including local geology, strain rate, and the stress state at the time of faulting (Ahlgren, 2001). Although the sequential development of shear surfaces within

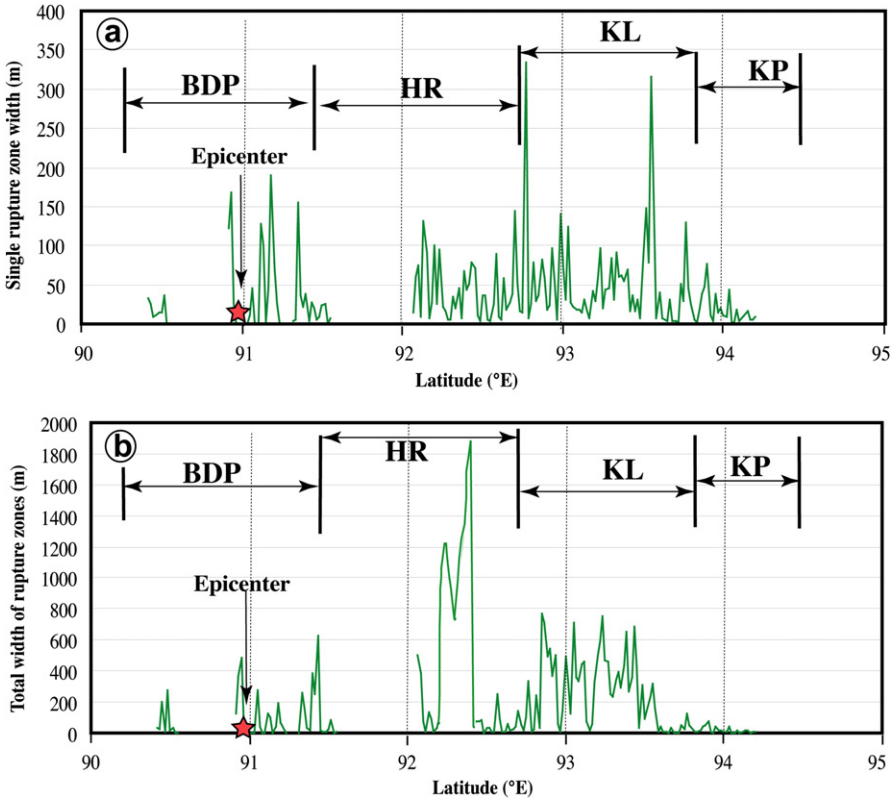

Fig. 5. Diagrams showing the widths of individual sub-rupture zones (a) and the total width of the entire rupture zone (b) within four segments along the fault. BDP: Buka Daban Peak segment; HR: Hongshui River segment; KL: Kusai Lake segment; KP: Kunlun Pass segment. The red star indicates the epicenter of the 2001 earthquake. (For interpretation of the references to colour in this figure legend, the reader is referred to the web version of this article.)

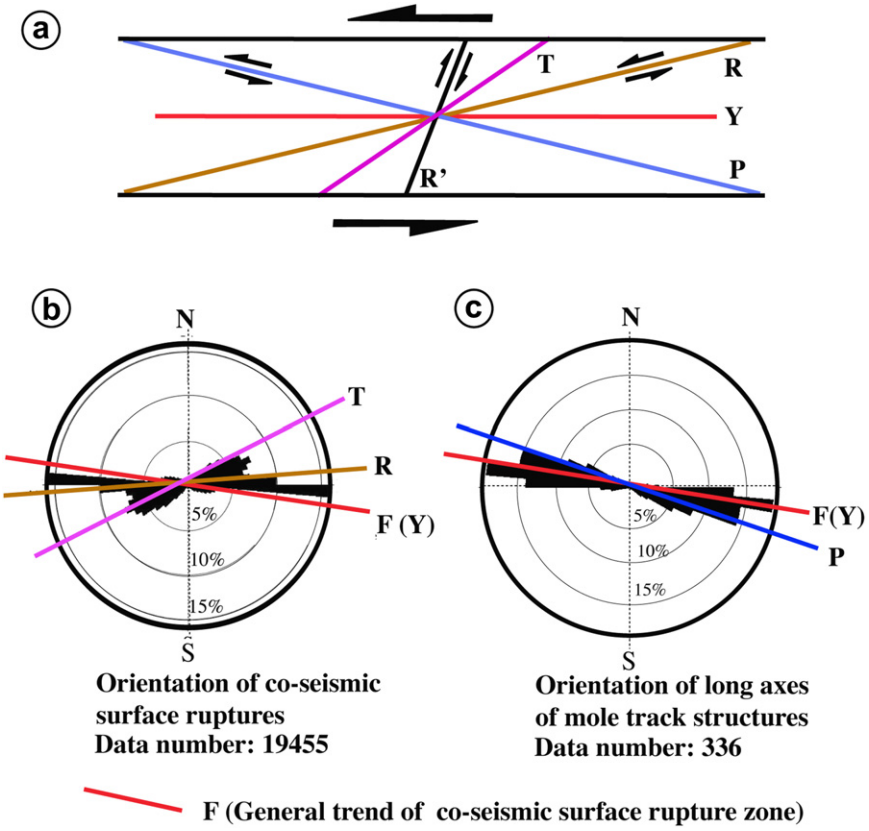

Fig. 6. Schematic diagram of a shear zone (a), rose diagrams showing the orientation of co-seismic surface rupture strands (b) and the orientation of fold axes of mole track structures (c), which together show the geometrical relationships between the main structural elements of the Riedel shear zone. Long arrows indicate the shear sense. (For interpretation of the references to colour in this figure legend, the reader is referred to the web version of this article.)

natural Riedel shear systems is still poorly understood, the most widely accepted model is based on *synthetic drivers* in the sense that lower-angle *R* and *P* shears generally pre-date higher-angle *R'* shears and *T* fractures (e.g., Morgenstern and Tchalenko, 1967; Bartlett et al., 1981; Davis et al., 1999; Ahlgren, 2001). The higher-angle Riedel shear geometries developed within the BDP and KL segments, and the lower-angle Riedel shears within the HR and KP segments (Fig. 4), may reflect the nature of local geological structures in unconsolidated alluvial deposits and basement rocks during co-seismic rupture formation. For example, the BDP and KL segments are located along a topographical boundary between a mountainous region and lowland basins filled with thick alluvial deposits, along which most of the surface ruptures associated with the 2001 event are new ruptures distributed in a zone up to 500 m wide (Lin et al., 2003). In contrast, the co-seismic surface ruptures in the HR segment are developed mainly within the pre-Mesozoic basement rocks along a narrow valley; in the KP segment, the ruptures occur mainly along a mountain range where co-seismic shear faults are developed in a narrow zone along pre-existing shear faults (Lin et al., 2003; Lin and Nishikawa, 2007).

The higher-angle *T* fractures can therefore be interpreted as new surface ruptures which developed mainly within unconsolidated alluvial deposits during the early stages of fault evolution (Fig. 8). In contrast, the lower-angle Riedel shears *R* and *Y* are new structures which developed in unconsolidated alluvial deposits and basement rocks, concentrated in a narrow zone that follows the pre-existing trace of the Kunlun Fault (Fig. 8). Accordingly, the Riedel shear structures related to the 2001 co-seismic surface ruptures consist of i) structures related to the strike-slip faulting, initiated within the unconsolidated alluvial deposits, and ii) reactivated pre-existing fault structures already present within the basement as a result of the earlier development of the fault.

The co-seismic Riedel shear structures described in this study are comparable with the previously-reported co-seismic strike-slip shear structures produced by large earthquakes, e.g., the 1912 M 7.1 earthquake (Bergerat and Angelier, 2003; Angelier et al., 2004; Gudmundsson, 2007) and the 2000 M 6.6 earthquake in South Iceland (Angelier and Bergerat, 2002), the 1920 M_S 8.7 Haiyuan earthquake in northeast Tibetan Plateau and the 1973 M_S 7.9 Luhuo earthquake in central-east Tibetan Plateau (Deng et al., 1986), the 1995 M_W 7.2 Kobe earthquake, Japan (Lin and Uda, 1996), and the 2010 M_W 6.9 Yushu earthquake in central Tibetan Plateau (Rao et al., in press). All these co-seismic strike-slip surface rupture zones are characterized by Riedel shear structures including en échelon tension cracks (*T* fractures), shear faults (*R* or *Y* shears), and mole tracks (or push-ups, *P* shears), which occurred within related pre-existing strike-slip fault zones. The co-seismic displacements were measured *in-situ* along the tension crack zones (*T* fractures) and shear faults (*R* or *Y* shears) along the co-seismic strike-slip surface rupture zones, as reported in the previous studies stated above, ranging from 1 m to 5 m in average (Deng et al., 1986; Lin and Uda, 1996; Lin et al., 2011) with a maximum amount of ~11 m produced by the 1920 Haiyuan earthquake (Deng et al., 1986), comparable with the co-seismic displacements produced by the 2001 event. In contrast, it is difficult to measure the co-seismic displacement *in-situ* along the mole track (or push-up) structures. Based on the deformation characteristics of mole track (push-up) structures, a maximum displacement of 2.4–2.67 m and a magnitude were inferred for related earthquakes along the strike-slip fault zones in South Iceland (Bergerat and Angelier, 2003; Angelier et al., 2004).

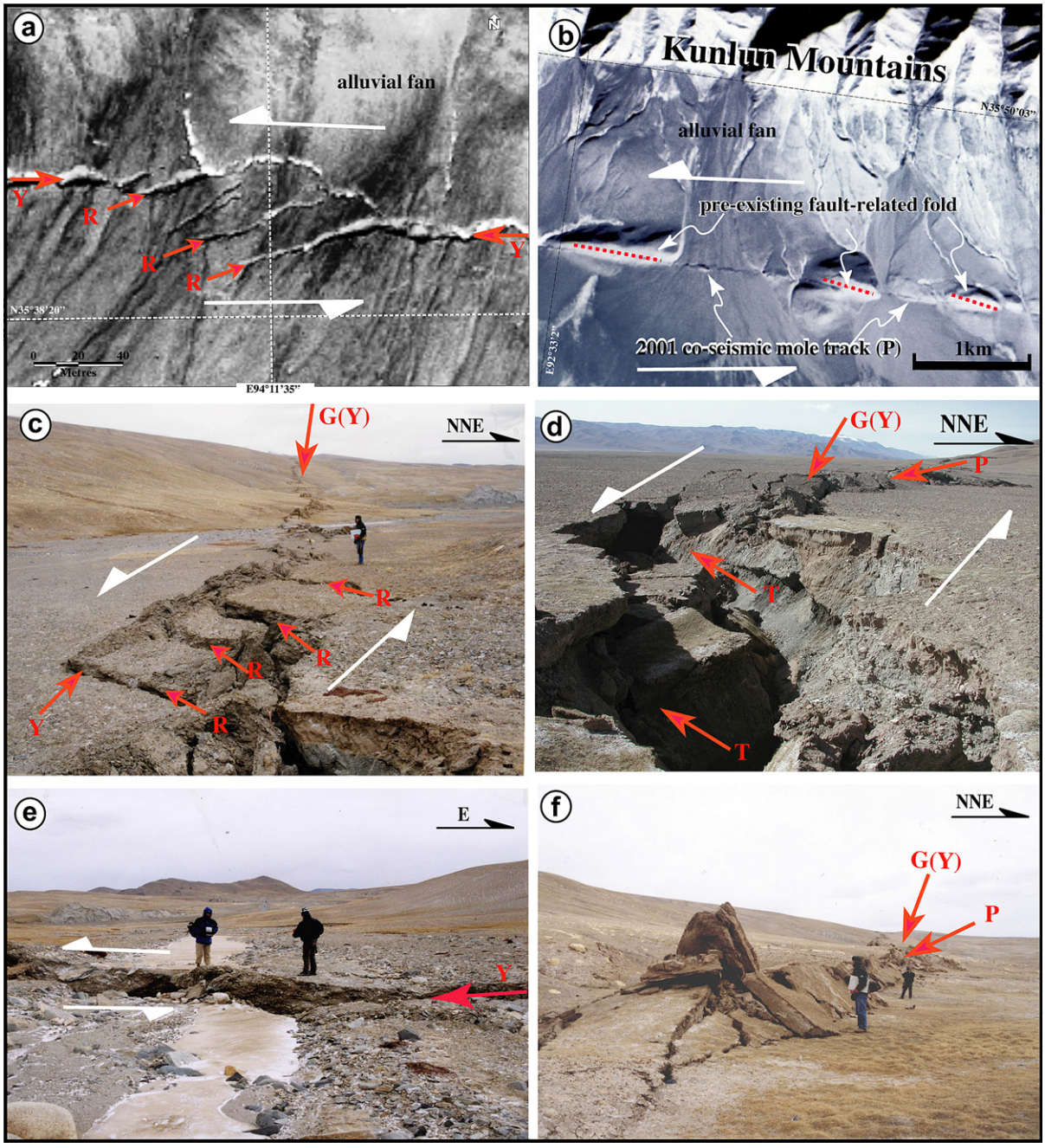

Fig. 7. IKONOS (a) and SPOT (b) images, and field photographs (c–f) showing the deformation features of co-seismic surface ruptures. (a) IKONOS image shows the right-hand en echelon pattern of *R* shears. (b) SPOT image showing the structural features of pre-existing and co-seismic mole track structures (*P* shears) (modified from Lin et al., 2004). The red dotted lines indicate the fold axes of pre-existing mole track structures. Note that the *P* shears show a left-hand en echelon pattern, indicating a left-lateral shear sense. (c) Photograph showing the right-hand en echelon *R* shears observed in the KP segment. (d) Photograph showing geometric features of the tension cracks (*T* fractures) and co-seismic mole track structures (*P* shears) observed in the KL segment. (e) Photograph showing the geometric features of the co-seismic shear fault (*Y* shear) observed in the KP segment. The small gully was offset ~2.5 m sinistrally. (f) Mole track structures observed in the KP segment. White arrows indicate a left-lateral shear sense. G(Y): general trend of the co-seismic surface rupture zone, parallel to *Y* shears. Long white arrows indicate the shear sense. (For interpretation of the references to colour in this figure legend, the reader is referred to the web version of this article.)

The present results, combined with the previous studies, confirm the fundamental importance of Riedel shear structures as common structures and quantitative indicators of co-seismic displacement within strike-slip shear zones, and show that Riedel shears are related to the early stages of fault formation. Furthermore, variations in the orientations of the various Riedel structures are a function of the magnitude and localization of shear strain, reflecting the different stages in the evolution of the shear zone (e.g., Ahlgren, 2001; Katz et al., 2004; Rao et al., in press).

5.2. Width of the co-seismic shear zone

Previous studies have shown that co-seismic surface ruptures produced by individual large-magnitude earthquakes are generally distributed throughout a zone ranging in width from several meters to several tens of meters (e.g., Lin and Uda, 1996; Yeats et al., 1997; Lin et al., 2001), although some such zones are up to 10 km in width (Lin et al., 2002, 2003). Geological and seismic data indicate that the sites of co-seismic surface ruptures are

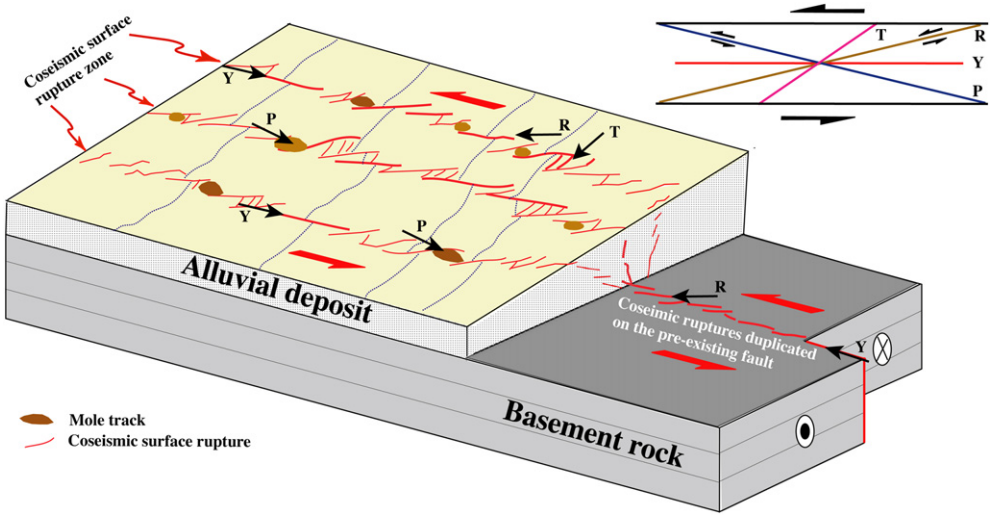

Fig. 8. Model for the formation of the co-seismic surface ruptures, showing the contrasting distribution patterns of co-seismic surface ruptures within unconsolidated alluvial deposits and within basement rock. See text for details.

controlled mainly by pre-existing fault zones (e.g., Yeats et al., 1997; Lin et al., 2002, 2003).

Field investigations carried out immediately after the 2001 Kunlun earthquake showed that the resulting co-seismic rupture zone is generally 5–50 m wide, although co-seismic extension cracks are locally found in an area as wide as 10 km, spaced at intervals of around 10 m (Lin et al., 2002, 2003). The measurements made during the present study indicate that the total width of a surface rupture zone is not uniform, and may vary along the four rupture segments from several meters up to 1890 m. The zone is generally wider in the KL segment and in part of the HR segment, where thick deposits of unconsolidated alluvial deposits are found, and the zone is thinner in the KP segment, which either lacks a covering of alluvium, or has just a thin covering (Fig. 5). The individual sub-rupture zones also show a tendency to be wider (up to 350 m) in the KL segment than in the KP segment (generally $<$100 m). The total width of the rupture zone is 3–10 times greater than that of individual sub-rupture zones, as measured in profiles across the surface rupture zone in the KL segment, whereas in the KP segment the total width is similar to that of individual sub-ruptures (Fig. 7). This finding indicates that the co-seismic surface ruptures in the KP segment are concentrated within a single zone.

As documented above, the co-seismic surface ruptures in the KL segment are mostly new fractures developed within alluvial deposits, and they are distributed over a wide area, whereas those in the KP segment are developed in a narrow zone within basement rocks. Accordingly, we conclude that i) the narrow co-seismic shear zone developed within basement is constrained by the pre-existing fault zone structure, and ii) the wider rupture zone, developed in unconsolidated alluvial deposits, is made up of several subparallel sub-rupture zones, with the geometry of a flower structure (Fig. 8).

6. Conclusions

On the basis of an analysis and interpretation of 1-m-resolution IKONOS and 0.61-m-resolution QuickBird images of the co-seismic surface rupture produced by the 2001 M_W 7.8 Kunlun earthquake on the Kunlun Fault, northern Tibet, we come to the following conclusions:

1) The co-seismic surface ruptures generally consist of Riedel shear structures, including *T* fractures, and *R*, *P*, and *Y* shears. These structures develop as a collection of up to five subparallel shear zones, where the individual zones vary in width from 3 m to 350 m (generally $<$100 m), and where the width across the entire rupture zone is generally $<$500 m (although locally up to 1890 m).
2) The lower-angle synthetic *R*, *P*, and *Y* shears are inclined at $<15^\circ$ and -10° to the general trend of the pre-existing Kunlun Fault, indicating a left-lateral shear sense.
3) The higher-angle *T* fractures are developed mainly within alluvial deposits, oriented at an angle of 15–40° to the general trend of the co-seismic rupture zone.

Our results confirm that Riedel shear structures are common within co-seismic surface rupture zones, and that they relate to the early stages of strike-slip fault evolution. Variations in the orientations of Riedel structural elements reflect the influence of pre-existing geological structures, representing different stages in the evolution of the shear zone, and reflect the magnitude and localization of shear strain.

Acknowledgments

We are grateful to Professors R. Caputo and A. Gudmundsson for critical reviews that helped to improve the manuscript and Professor K. Kano for discussion and comments throughout this study. This work was supported by the Science Project (Project No. 23253002 for A. Lin) of the Ministry of Education, Culture, Sports, Science and Technology of Japan.

References

Ahlgren, S.G., 2001. The nucleation and evolution of Riedel shear-zones as deformation bands in porous sandstone. Journal of Structural Geology 23, 1203–1214.
Angelier, J., Bergerat, F., 2002. Behaviour of a rupture of the June 21 2000, earthquake in South Iceland as revealed in an asphalted car park. Journal of Structural Geology 24, 1925–1936.
Angelier, J., Bergerat, F., Bellou, M., Homberg, C., 2004. Co-seismic strike-slip fault displacement determined from push-up structures: the Selsund Fault case, South Iceland. Journal of Structural Geology 26, 709–724.
Bartlett, W.L., Friedman, M., Logan, J.M., 1981. Experimental folding and faulting of rocks under fonfining pressure. Part IX, Wrench faults in limestone layers. Tectonophysics 79, 255–277.

Bergerat, F., Angelier, J., 2003. Mechanical behaviour of the Arnes and Hestfjall Faults of the June 2000 earthquakes in Southern Iceland: inferences from the surface traces and tectonic model. Journal of Structural Geology 25, 591–609.
Cunningham, W.D., 1993. Strike-slip faults in the southernmost Andes and the development of Patagonian orocline. Tectonics 12, 169–186.
Davis, G.H., Bump, A.P., Garcia, P.E., Ahlgren, S.G., 1999. Conjugate Riedel deformation band shear-zones. Journal of Structural Geology 22, 169–190.
Deng, Q., Wu, D., Zhang, P., Chen, S., 1986. Structure and deformational character of strike-slip fault zones. Pure and Applied Geophysics 124, 203–223.
Fu, B., Lin, A., 2003. Spatial distribution of the surface rupture zone associated with the 2001 M_S 8.1 Central Kunlun earthquake, northern Tibet, revealed by satellite remote sensing data. International Journal of Remote Sensing 24, 2191–2198.
Gudmundsson, A., 2007. Infrastructure and evolution of ocean-ridge discontinuities in Iceland. Journal of Geodynamics 43, 6–29.
Guo, J., Lin, A., Maruyam, T., Zheng, J., Sun, G., 2006. New constraints on recent large earthquakes along the Xidatan-Dongdatan segment of the Kunlun fault, western China. Bulletin of Seismological Society of America 96, 48–58.
Guo, J., Lin, A., Su, G., Zheng, J., 2007. The 1937 M7.5 earthquake and paleoseismicity along the Tuosuo lake segment of the Kunlun fault, northern Tibet, China. Bulletin of Seismological Society of America 97, 474–496.
International Seismological Centre, 2001. On-line Bulletin. www.isc.ac.uk/Bull (last accessed June 2010).
Jia, Y., Dai, H., Su, X., 1988. In: Xinjiang Seismological Bureau (Ed.), Tuosuo Lake earthquake fault in Qinghai province, in Research on Earthquake Faults in China. Xinjiang People Press, Urumqi, China, pp. 66–71 (in Chinese).
Katz, Y., Weinberger, R., Aydina, A., 2004. Geometry and kinematic evolution of Riedel shear structures, Capitol Reef National park, Utah. Journal of Structural Geology 26, 491–501.
King, G., 1986. Speculations on the geometry of the initiation and termination process of earthquake rupture and relation to morphology and geological structures. Pure and Applied Geophysics 124, 567–586.
Lin, A., Guo, J., 2008. Non-uniform slip rate and millennial recurrence interval of large earthquakes along the eastern segment of the Kunkun Fault, northern Tibet. Bulletin of Seismological Society of America 98, 2866–2878. doi:10.1785/0120070193.
Lin, A., Guo, J., 2009. Pre-historic large earthquake inferred from liquefaction along the Kusai Hu segment of the Kunlun fault, northern Tibet. In: The Geological Society of London, Special Publications, vol. 316. doi:10.1144/SP316.8, pp. 145–154.
Lin, A., Nishikawa, M., 2007. Coseismic lateral offsets of surface rupture zone produced by the 2001 Mw 7.8 Kunlun earthquake, Tibet from the IKONOS and QuickBird imagery. International Journal of Remote Sensing 28, 2431–2445. doi:10.1080/01431160600647233.
Lin, A., Uda, S., 1996. Morphological characteristics of the earthquake surface ruptures occurred on Awaji Island, associated with the 1995 Southern Hyogo Prefecture Earthquake. The Island Arc 5, 1–15.
Lin, A., Fu, B., Guo, J., Zeng, Q., Dang, G., He, W., Zhao, Y., 2002. Coseismic strike-slip and rupture length produced by the 2001 Ms 8.1 Central Kunlun earthquake. Science 296, 2015–2017.
Lin, A., Guo, J., Fu, B., 2004. Co-seismic mole-track structures produced by the 2001 Ms 8.1 Central Kunlun earthquake, China. Journal of Structural Geology 26, 1511–1519.
Lin, A., Guo, J., Awata, Y., Kano, K., 2006. Average slip rate and recurrence interval of large magnitude earthquakes on the western segment of the Kunlun fault, northern Tibet. Bulletin of Seismological Society of America 96, 1597–1611.
Lin, A., Kikuchi, M., Fu, B., 2003. Rupture segmentation and process of the 2001 M_w 7.8 central Kunlun earthquake, China. Bulletin of Seismological Society of America 93, 2477–2492.
Lin, A., Ouchi, T., Chen, A., Maruyama, T., 2001. Co-seismic displacements, folding and shortening structures along the Chelungpu surface rupture zone occurred during the 1999 Chi-Chi (Taiwan) earthquake. Tectonophysics 330, 225–244.
Lin, A., Rao, G., Jia, D., Wu, X., Yan, B., Ren, Z., 2011. Co-seismic strike-slip surface rupture and displacement produced by the 2010 Mw 6.9 Yushu earthquake, China, and implications for Tibetan tectonics. Journal of Geodynamics 52, 249–259.
Lin, A., Ren, Z., Jia, D., Wu, X., 2009. Co-seismic thrusting rupture and slip distribution produced by the 2008 Mw7.9 Wenchuan earthquake, China. Tectonophysics 47, 203–215. doi:10.1016/j.tecto.2009.02.014.
Molnar, P., Tapponnier, P., 1975. Cenozoic tectonics of Asia: effects of a continental collision. Science 189, 419–426.
Morgenstern, N.R., Tchalenko, J.S., 1967. Microscopic structures in kaolin subjected to direct shear. Geotechnique 17, 309–328.
Moore, J.M., 1979. Tectonics of the Najad transcurrent fault system, Saudi Arabia. Journal of Geological Society of London 136, 441–452.
Naylor, M.A., Mandl, G., Sijpesteijn, C.H.K., 1986. Fault geometries in basement-induced wrench faulting under different initial stress states. Journal of Structural Geology 8, 737–752.
Peltzer, C., Crampe, F., King, H., 1999. Evidence of nonlinear elasticity of the crust from the Mw 7.6 Manyi earthquake. Science 286, 272–276.
Rao, G., Lin, A., Jia, D., Wu, X., Yan, B., Ren, Z. Co-seismic surface strike-slip shear structures produced by the 2010 Mw6.9 Yushu earthquake, central Tibetan Plateau. Tectonophysics, in press, doi:10.1016/j.tecto.2011.05.011.
Riedel, W., 1929. Zur Mechanik Geologischer Brucherscheinungen. Zentral-blatt fur Mineralogie. Geologie und Paleontologie B, 354–368.
Tapponnier, P., Xu, Z., Roger, F., Meyer, B., Arnaud, N., Wittinger, G., Yang, J., 2001. Oblique stepwise rise and growth of the Tibet plateau. Science 294, 1671–1677.
Tchalenko, J.S., 1968. The evolution of kink-bands and the development of compression textures in sheared clays. Tectonophysics 6, 159–174.
Tchalenko, J.S., 1970. Similarities between shear-zones of different magnitudes. Geological Society of America Bulletin 81, 1625–1640.
Tchalenko, J.S., Ambraseys, N.N., 1970. Structural analysis of the Dasht-eBayaz (Iran) earthquake fractures. Geological Society of America Bulletin 81, 41–60.
Yeats, R.S., Sieh, K., Allen, C.R., 1997. The Geology of Earthquake. Oxford University Press, Oxford.
Zhang, P., Shen, Z., Wang, M., Gan, W., Buergmann, R., Molnar, P., Wang, Q., Niu, Z., Sun, J., Wu, J., Sun, H., You, X., 2004. Continuous deformation of the Tibetan plateau from Global positioning system data. Geology 32, 809–812.